THE JOURNAL OF PHYSICAL CHEMISTRY C

Article

Cite This: J. Phys. Chem. C 2019, 123, 15618−15628

pubs.acs.org/JPCC

Sodium Halide Adsorption and Water Structure at the α-Alumina(0001)/Water Interface

Published as part of The Journal of Physical Chemistry virtual special issue "Hai-Lung Dai Festschrift".

Ruiyu Wang,[†,‡] Mark DelloStritto,[†,‡,§] Richard C. Remsing,[†,‡,§] Vincenzo Carnevale,*[,§,∥] Michael L. Klein,[†,‡,§] and Eric Borguet*[,†,‡]

[†]Department of Chemistry, Temple University, Philadelphia, Pennsylvania 19122, United States

[‡]Center for Complex Materials from First-Principles (CCM), Temple University, 1925 North 12th Street, Philadelphia, Pennsylvania 19122, United States

[§]Institute for Computational Molecular Science, Temple University, Philadelphia, Pennsylvania 19122, United States

[∥]Department of Biology, Temple University, Philadelphia, Pennsylvania 19122, United States

Supporting Information

ABSTRACT: Alumina is one of the most abundant minerals and has a wide range of industrial applications, with catalysis as one of the most important. Of particular relevance for catalysis is the structure of the mineral/water interface. In this work, water structure and sodium halide adsorption at the neutral α-alumina(0001)/water interface are investigated using molecular dynamics simulations. This work demonstrates the accuracy of the chosen model of the alumina/water interface and shows that high charge density monovalent ions, such as Na^+ and F^-, have a strong affinity for the interface due to the specific pattern of alumina surface OH groups, such that the adsorbed ions displace waters that are hydrogen-bonded to the surface in their absence. A significant portion of the driving force for anion adsorption arises from surface bound Na^+, which reverse the intrinsic surface dipole field and drive the accumulation of halides at the interface. The resulting electrolytic interfacial structure reorients water molecules as far as 1 nm from the surface. Although ion adsorption does not alter the global orientation of surface OH groups, it significantly affects their local geometry. This in turn may affect the reactivity of surface groups and thus play a role in chemical processes occurring at the interface.

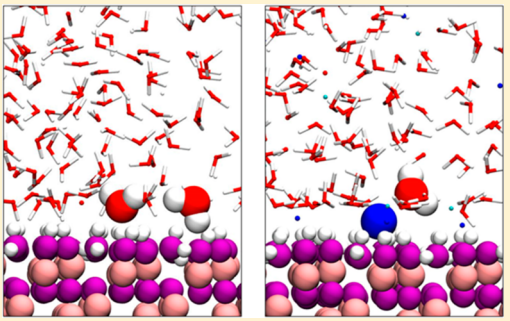

INTRODUCTION

Water−mineral interfaces are ubiquitous and have been shown to drive diverse chemical processes, including the erosion of rocks,[1] harvesting of energy from sun light,[2] and prebiotic chemistry.[3] In particular, alumina (Al_2O_3), an earth-abundant aluminum oxide, is used in industry due to its chemical and physical stability.[4] For example, activated alumina plays an important role in catalytic applications, including the polymerization of methyl methacrylate[5] and peptide bond formation.[6] Porous activated alumina is widely used to purify water by removing fluoride and arsenic ions from aqueous solution.[7] Alumina is also used as a desiccant because of its strong affinity for water.[8] In each of these applications, the interface between aqueous solution and the alumina surface dictates performance. Despite their importance, many fundamental questions regarding mineral−water interfaces remain unanswered. For instance, the precise interplay among surface chemistry, interfacial water structure and ion adsorption remains poorly characterized.[9]

The interaction between pure water and the alumina surface has been previously examined.[10−13] Though informative, experimental approaches such as high-resolution specular X-ray reflectivity (XRR),[14] atomic force microscopy,[15] and vibrational sum frequency generation (vSFG) spectra[16−19] provide only indirect information about the surface properties. A model of the surface structure is needed to fit and interpret the experimental results. On the other hand, molecular dynamics (MD) simulations provide detailed structural information but are limited in scope due to inherent approximations and time- and length-scale limitations. Hence, a coupling between computation and experiments whereby molecular simulations are first validated and then used to provide a microscopic interpretation of the experimental results is one of the most effective strategies to study complex molecular phenomena occurring at water−mineral interfaces.

A particularly relevant question concerns the distribution of ions at the water−alumina interface.[20,21] This property is

Received: April 1, 2019
Revised: May 18, 2019
Published: June 13, 2019

DOI: 10.1021/acs.jpcc.9b03054
J. Phys. Chem. C 2019, 123, 15618−15628

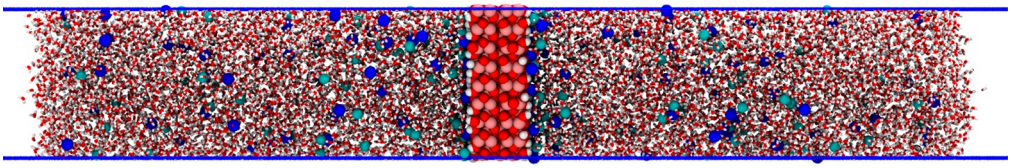

Figure 1. Snapshot of the classical MD simulation box. The simulation box is symmetric with the alumina in the middle. Two water−air interfaces are created to maintain the pressure at that of water−vapor coexistence. The color scheme is as follows: pink, Al; red, O; white, H; blue, Na; green, halide ion.

difficult to characterize using experiments alone. In this work, classical MD simulations are employed to investigate the α-alumina(0001)/aqueous electrolyte interface. The focus is on α-alumina (corundum) because it is the thermodynamically stable phase of alumina at ambient conditions.[22] To quantify the adsorption of sodium halides and how ion adsorption affects interfacial water structure, several models of alumina based on the CLAYFF force field are investigated and simulations based on a flexible solid surface combined with appropriate Al−O−H angle bending potentials lead to a surface model that is consistent with ab initio MD (AIMD) simulations and experimental results. After establishing the accuracy of this model, simulations show that ions with high charge density, such as Na^+ and F^-, have a strong affinity for the alumina(0001) surface, with cooperative effects playing an important role. Ion adsorption also affects water structure at the surface, decreasing the relative population of water molecules donating a hydrogen bond to the surface and increasing the relative population of water molecules associated with the hydration shell of Na^+. As a result, the average orientation of water molecules near the interface changes direction and increases in magnitude upon addition of salts. This effect is more pronounced for NaI than NaF solutions, indicating NaI orders water more than NaF. Such behavior originates from the ability of F^- to screen the electric field generated by the adsorbed excess Na^+ more effectively than I^-, arising from an interplay between solvation and interfacial electrostatics. In the Conclusion, the impact of this work on the understanding of chemistry at water−mineral interfaces is also discussed.

SIMULATION METHODOLOGY AND SURFACE MODEL

Simulation Details and Data Analysis. In this work, the solid α-alumina(0001) surface coordinates are described by Scardi,[23] and a fully hydroxylated and neutral surface is applied to investigate the α-alumina (0001)/water interface at pH 7. The thickness of the alumina solid is about 1 nm, so that water molecules on either side do not interfere with each other. Classical MD simulations were carried out using GROMACS 2016.3.[24−30] The solid alumina was modeled using the CLAYFF force field.[31] The force field parameters for the ions were developed by Netz and co-workers to reproduce the ion solvation free energy, solvation entropy, and the position of the first peak of the radial distribution function.[32] The water model is the SPC/E model, which was used in the parametrization of the CLAYFF force field and reproduces the bulk and interfacial properties of water at ambient conditions with good accuracy.[33] Water bonds and angles are held fixed using the LINCS algorithm.[34] Simulations of a fully flexible surface were performed in the $NP_{XY}L_ZT$ ensemble, where constant pressure is maintained in the X and Y directions while the length of the Z-direction, L_Z, is held fixed. The pressure is maintained at 1 bar using the Parrinello−Rahman barostat for the production simulations.[35,36] The temperature is maintained at 300 K using a Nosé−Hoover thermostat with a relaxation time of 0.1 ps.[37,38] A water/vacuum interface in the Z direction of the simulation box is created to maintain the simulation at the pressure of water−vapor coexistence (Figure 1). Short-ranged interactions are cut off at 1 nm. Long-ranged electrostatics are evaluated with the particle−mesh Ewald method.[39] The resulting simulation box is approximately L_X = 3.8 nm and L_Y = 3.3 nm, and L_Z is fixed at 40 nm and contains 8788 water molecules.

To study ion behavior, sodium halide ion pairs are randomly inserted to make the salt concentration in the bulk equal to 0.75 M on each side of the solid in the simulation box. The leapfrog algorithm was used to integrate the equations of motion with a time step of 1 fs. Equilibration was considered to be achieved when the ion number density near the solid interface no longer changes with time. Following equilibration, production simulations for data collection were run for an additional 50 ns.

The number density profile and the water polar orientation were obtained by the GROMACS built-in tools *gmx density* and *gmx h2order*, respectively, along the Z direction. The water density profile is represented by the water oxygen atom density distribution. The electric field was calculated by the tool *gmx potential*, which integrates Poisson's equation using the charge density profile. The bin size of such profiles is 0.05 Å. The surface OH orientation distribution, the water dipolar angle (orientation) distribution, the ion coordination interaction near the surface, and the average position of the surface oxygen atoms were analyzed with the MDAnalysis library.[40,41] For the density profile of ions and the water orientation, the data reported is averaged over both sides of the simulation cell. The potentials of mean force (PMFs) are obtained using umbrella sampling.[42] All umbrella sampling simulations were performed using PLUMED[43] and free energies were reconstructed using UWHAM.[44] All snapshots were generated by the VMD software.[45]

Car−Parrinello AIMD simulations were performed using Quantum Espresso (QE) v.6.2.1.[46,47] The PBE-based HSCV pseudopotentials are used and the valence electrons are treated explicitly.[48] Density functional theory based electronic structure calculations were performed using the strongly constrained and appropriately normed (SCAN) functional,[49] which has been shown to accurately reproduce a variety of covalent and noncovalent interactions,[50] including those in bulk water[51] and alumina/water interfaces.[52] The simulations cells were initialized using CLAYFF with the z-lattice reduced from 12 to 3.5 nm at 423 K to 3.5 nm over 1 ns, followed by a temperature reduction to 300 K for 1 ns and equilibration at 300 K for 1 ns. The electron mass is set to 100 au and the time

DOI: 10.1021/acs.jpcc.9b03054
J. Phys. Chem. C 2019, 123, 15618−15628

step is set to 2.0 au, and a plane-wave cutoff of 90 Ry was used.[12,13] Each of five independent simulations were equilibrated using QE in the *NVT* ensemble until the total energy and temperature were converged and then run in the *NVE* ensemble for 27.5 ps. Each unit cell has dimensions of (0.824 × 0.952 × 3.5) nm and includes 6 alumina layers, 12 aluminol groups per surface, and 52 H_2O molecules, resulting in a water density of 0.998 g/cm^3 and the thickness of water layer is roughly 2 nm. The AIMD electron density is calculated by averaging over 15 frames, taken from each of the five independent AIMD trajectories (three each). Further averaging over the $x-y$ plane was then performed to yield the electron density profile along the Z direction.

Alumina Surface Model. The classical MD simulation box consists of a slab of alumina(0001) surrounded by water molecules on each side and a vacuum region (Figure 1). Previous low energy electron diffraction,[53,54] X-ray methods,[55,56] dynamic-mode scanning force microscopy[57] and MD simulations[22,58] revealed that when the alumina(0001) surface meets water, dissociative adsorption is more favorable than associative adsorption. This transforms terminal Al atoms to Al−O−H species, resulting in a fully hydroxylated α-alumina(0001) surface.[59] As a result, the alumina surface is fully hydroxylated in all simulations of this work.

The accuracy of classical models depends on the choice of force field parameters. In this work, the CLAYFF force field, which reproduces many of the relevant properties of minerals, is used.[31] The original CLAYFF force field contains a surface metal−O−H angle bending potential, but many studies omit this term.[31] However, the orientational preferences of surface OH groups have been shown to impact interfacial processes.[60] A recent ab initio MD study found two favored surface O−H orientations: an "out-of-plane" one in which the OH groups are perpendicular to the alumina surface and an "in-plane" one in which OH groups are nearly parallel to the alumina surface plane.[61] An accurate force-field should reproduce this distribution of hydroxyl group orientations. Therefore, we tested how the inclusion of the Al−O−H bending potential affected the results and the classical MD simulations with Al−O−H bending potentials predicted a distribution of OH orientations in agreement with the results from AIMD by SCAN, as shown in Figure 2. Although simulations that omit this bending term still reproduce this feature to some extent, the distribution of OH orientations is less ordered and the probability of intermediate orientations, e.g., at θ_{OH} = 60°, is overestimated (Figure 2). Accurately modeling this distribution of OH orientations is important for describing ion adsorption, as discussed further in the Supporting Information.

The electron density of interfacial water is also compared with XRR experiments and AIMD simulations by the SCAN functional (Figure 3). The classical electron density is calculated by convoluting the water oxygen density with a Gaussian function that has a standard deviation of one-third of oxygen atom van der Waals (VDW) radius (0.0507 nm).[62,63] The idea is that all water electrons are assumed to be on the oxygen atom and most are distributed within the oxygen's VDW radius in a Gaussian form. The XRR reference is fitted from XRR spectra as described in Catalano's paper.[14]

The electron densities from experiment, AIMD, and classical MD are shown in Figure 3. The classical electron density reproduces the first peak of the experimental distribution, with the AIMD results having a slightly larger intensity. The positions of the remaining peaks are in good agreement, with

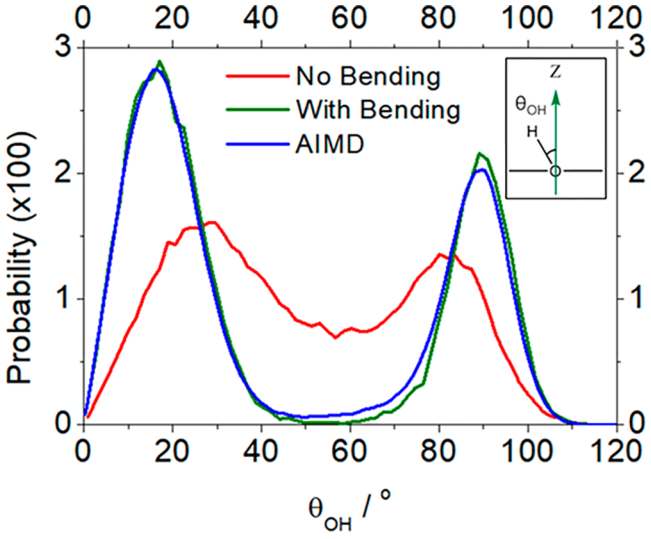

Figure 2. Probability distribution of the angle, θ_{OH}, made by surface OH groups and the surface normal (positive direction of Z axis), as shown in the inset. The green curve is a classical MD simulation using a flexible surface with the Al−O−H bending term, which overlaps well with data from AIMD simulation by SCAN functional (blue curve). The red curve is from a classical MD simulation without the bending term.

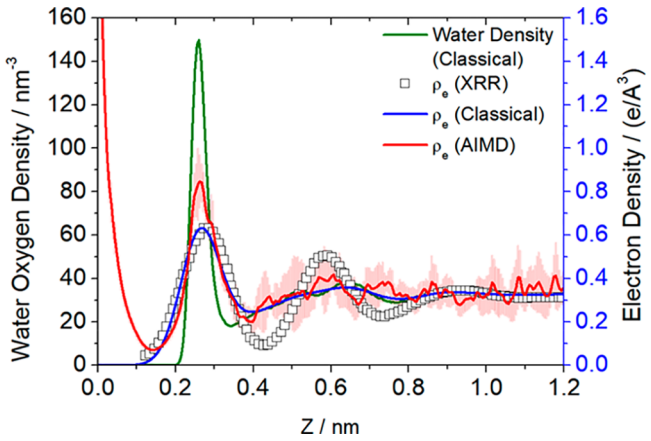

Figure 3. Water density profile (scale on the left) and electron density profile (scale on the right). The water density profile is calculated by counting the water oxygen as described in the main text. The experimental result is from Catalano.[14] Methods for calculating simulated spectra from both classical and AIMD simulations are described in the simulation detail section. Details of the water density profile are discussed in the text. Light red shade shows the error bar, 1 standard deviation, of the electron density by AIMD.

AIMD and classical MD predictions in quantitative agreement with each other with respect to the peak intensities. The experimentally estimated electronic density indicates significant layering at the alumina/water interface, evidenced by the deep first and second minima, as well as a large second peak height. Such significant structuring in this range is not observed in either the classical MD or the AIMD simulations. This difference is attributed to uncertainties within the fitting of the electron density from the XRR spectra; a range of densities can be consistently fit to the same spectra.[64] The good agreement of electron densities between AIMD and the classical MD predictions, combined with the reasonable agreement with the peak positions estimated from experiments,

DOI: 10.1021/acs.jpcc.9b03054
J. Phys. Chem. C 2019, 123, 15618−15628

suggests that the classical model used here provides an accurate representation of the alumina/water interface.

RESULTS AND DISCUSSION

Ion Adsorption. Next, simulations in the presence of sodium halides NaF, NaCl, NaBr, and NaI are carried out and ion adsorption to the alumina(0001)/water interface is quantified. The halide number density near the solid surface is significantly larger than that of the bulk for all anions (Figure 4a), indicating a high propensity for ion adsorption at the

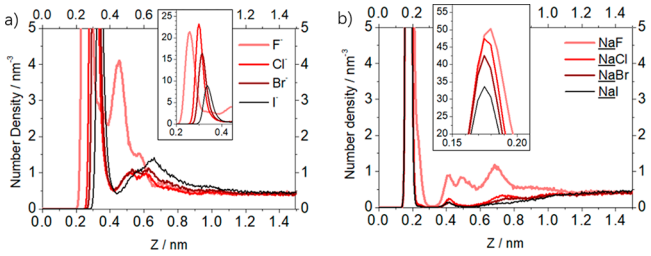

Figure 4. Number density of ions versus distance from the alumina surface in each simulation with sodium halides. The number density at the bulk is about 0.45 nm^{-3}, corresponding to 0.75 M solution for all ions. $Z = 0$ is defined by the average positions of the surface oxygen atoms of alumina. Key: (a) number density of halides; (b) number density of Na^+.

alumina surface. The relative adsorption propensity of each halide is proportional to their charge density, with the highest charge density ions adsorbing the most, opposite to what is observed at the water−vapor and other hydrophobic interfaces.[65−76]

To quantify this propensity for the surface, the Z-dependent adsorption is calculated (Figure 5a)

$$\Gamma(Z) = \int_0^Z [1 - H(Z' - Z_{GDS})] \times [\rho(Z') - \rho(0)]\, dZ' + \int_0^Z H(Z' - Z_{GDS}) \times [\rho(Z') - \rho(\infty)]\, dZ' \quad (1)$$

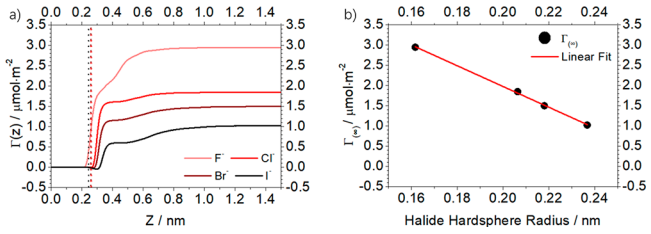

Figure 5. (a) Adsorption $\Gamma(Z)$ of halides in each simulation. The vertical dash lines are the Gibbs dividing surfaces of each simulation. (b) Linear fitting of adsorption $\Gamma(\infty)$ as a function of the halide effective hard sphere radius.

where $\rho(Z)$ is the number density of the ion of interest at a distance Z from the surface, $\rho(\infty)$ is the bulk concentration obtained by averaging over the bulk solution region of the simulation box, and $H(x)$ is the Heaviside step function. Z_{GDS} is the position of the Gibbs dividing surface, which is defined as the surface that yields $\Gamma_{water}(\infty) = 0$. Physically, $\Gamma(\infty)$ corresponds to the excess number of ions at the surface relative to the bulk per unit area. The adsorption, $\Gamma(Z)$, transitions from zero to a plateau at $\Gamma(\infty)$ where the system reaches the bulk concentration. For the larger halides, a slight negative minimum near the GDS is observed, indicating local depletion of the anion near the GDS, although the total adsorption is positive. The $\Gamma(\infty)$ and halide effective hard sphere radius are linear dependent as shown in Figure 5b, where the hard sphere radius was estimated following previous work.[77,78] This suggests that the adsorption of monovalent halides is determined by their size or, equivalently, their charge density.

Experimental adsorption measurements of fluoride have found that $\Gamma(\infty) = 4.5$ and 2.13 μmol/m^2 for F^- at pH 7.0 and pH 9.0, respectively, at 25 °C.[79] The experimental work studied adsorption to alumina powder, whose point of zero charge (PZC) was determined to be pH 9.0. The PZC of alumina(0001) has been measured to be at approximately pH 7.[19] Since both pH and surface charge are anticipated to impact F^- adsorption to alumina, and 2.9 μmol/m^2, which was predicted from simulations, is within the above experimental range, this further supports the accuracy of the model for the aqueous electrolyte−alumina interface. Note that omission of the Al−O−H angle bending potential results in a smaller estimate of $\Gamma(\infty) \approx 2.6$ μmol/m^2, as shown in the Supporting Information, highlighting the sensitivity of macroscopic thermodynamic quantities to subtle details of the alumina−water interface model.

It is not surprising that sodium cations approach closer to the surface than halides, because Na^+ is smaller and can directly bind to the oxygen atoms of the surface. In each simulation, the number density of Na^+ near the interface is larger than that of the counterion (Figure 4b). Interestingly, the interfacial Na^+ number density increases as the charge density of the counterion increases. This dependence of Na^+ adsorption on the nature of the counterion suggests that collective effects play an important role in determining the adsorption of ions to the surface.

It is difficult to disentangle the direct interaction of an ion with the surface from indirect effects due to co- and counterions. In an effort to separate these effects, potentials of mean forces (PMFs) for ion adsorption at the finite bulk concentration of 0.75 M, from the number densities in Figure 4, and in the limit of a single ion (in this work, concentration of one ion is 0.0125 M) by umbrella sampling are calculated. The single ion PMF differs from that of the finite concentration solution (Figure 6) due to direct and indirect ion−ion interactions.

For Na^+, the free energy of single ion adsorption relative to the bulk is about $10kT$, corresponding to the depth of the first minimum in the PMF, where T is the temperature and k is Boltzmann's constant. This large free energy difference suggests that Na^+ establishes favorable interactions with the surface. When the concentration of the solution is increased, this adsorption free energy is decreased to approximately the same value for all anions. Thus, collective effects tend to disrupt the adsorption of Na^+ directly to the surface. However, further structuring of the PMF away from the surface depends on the identity of the counterion, and this is discussed in the next section.

The free energy of adsorption for a single F^- or Cl^- is about $2kT$, and that for I^- is nearly zero. This is in stark contrast with the results from simulations of 0.75 M solutions, for which halides have a free energy of adsorption between approximately $3kT$ and $4kT$. This suggests that collective effects tend to enhance the adsorption of anions to the alumina surface.

DOI: 10.1021/acs.jpcc.9b03054
J. Phys. Chem. C 2019, 123, 15618−15628

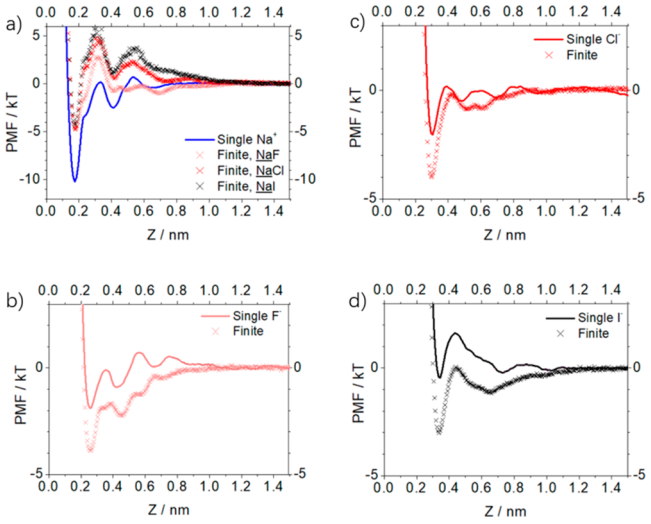

Figure 6. PMFs for adsorption of (a) Na^+, (b) F^-, (c) Cl^-, and (d) I^-. Curves marked as "Finite" are calculated from simulations with 0.75 M ions. The single ion PMFs were computed from umbrella sampling simulations with a single ion in water.

Halide adsorption is driven by attractive electrostatic interactions with Na^+ ions bound to the alumina surface. Excess Na^+ at the interface creates a positive electric field, preventing further Na^+ adsorption; see the Supporting Information. Adsorption of high charge density halides into the interfacial region partially screens the electric field generated by Na^+, thereby enabling adsorption of additional Na^+ ions (Figure 4). Similar cooperative effects have also been suggested to play a role in biomolecule adsorption to alumina,[80,81] and our findings suggest that these interactions case be tuned through varying the identity of the anion, in addition to altering the nature of cation adsorption.

Coordination Structure of Adsorbed Ions. Snapshots of the interface illustrate the reason for the high surface affinity of ions (Figure 7). Due to the specific hexagonal pattern of

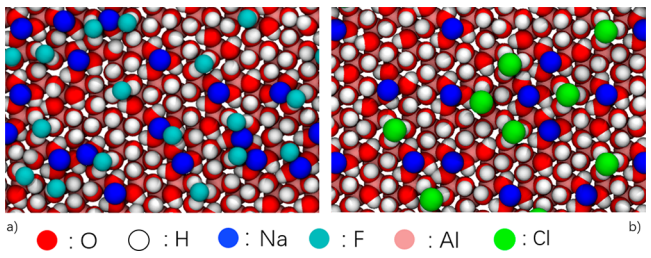

Figure 7. Snapshot of (a) NaF and (b) NaCl adsorption near the α-alumina(0001)/water interface. Water molecules are omitted for clarity. Pink, red, white, blue, dark green, and light green spheres represent aluminum, oxygen, hydrogen, sodium, fluorine, and chlorine atoms, respectively. In both simulations, most Na^+ ions are triply coordinated by the surface, and halides can form H-bonds with hydroxyl groups of the surface.

aluminum atoms and the resulting triangular pattern of surface OH groups, the α-alumina (0001) surface can substitute part of the ion hydration shell with up to three surface hydroxyl groups when an ion adsorbs to the surface. In particular, Na^+ can interact with three surface oxygen atoms in a triangular adsorption site, while halides can accept between 1 and 3 hydrogen bonds on average from surface hydroxyl groups, depending on the nature of the ion. However, these structures are not rigid, and structural fluctuations both of the solution and of the solid surface result in distributions of coordination structures.

To quantify these fluctuations, the distributions of coordination numbers of, and hydrogen bonds to, ions adsorbed at the alumina/water interface are computed (Figure 8). An ion, water, or surface hydroxyl is considered to be

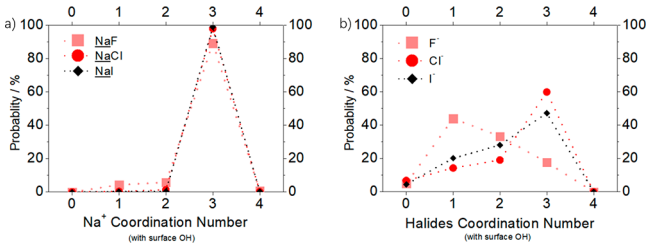

Figure 8. (a) Probability distributions of the number of alumina hydroxyl groups coordinated to sodium cations and (b) probability distributions of hydrogen bonds formed between alumina hydroxyl groups and halide ions. All probability distributions are evaluated for ions within the first peak of their respective density profiles.

within the first coordination shell of an ion if the distance is less than that of the first minimum in the respective pair distribution function. The coordination number distributions for Na^+ are sharply peaked at three, suggesting that nearly all adsorbed cations at the solid surface are triply coordinated by hydroxyl oxygens (Figure 8a), in a rigid environment that allows only minimal fluctuations away from this maximum coordination number.

In the case of halides, distributions of hydrogen bonds accepted from water and surface hydroxyl groups are analyzed. The definition of an H-bond is when the $O-X^-$ and $H-X^-$ distances are less than the position of the first minimum in the radial distribution function, and the corresponding $H-O-X^-$ angle is smaller than 30°, where X^- indicates a halide.[82−84] The distributions of hydrogen bonds accepted by surface-adsorbed halides are shown in Figure 8b. Due to the orientational freedom of the surface hydroxyl groups, the coordination structure of adsorbed halides is much less rigid than that observed for sodium ions. Each halide hydrogen bond distribution exhibits a single peak—at one for F^- and three for other halides—in addition to significant probabilities of coordination structures other than the peak. This indicates that the coordination environment of the halides is significantly more dynamic and flexible than that of the adsorbed sodium ions.

In addition, fluoride behaves differently than the remaining halides. The predominant binding mode of F^- involves a single hydrogen bond, while the remaining halides typically accept three H-bonds. Examples of these structures can be observed in the snapshots in Figure 7, highlighting $F^-{-}Na^+$ ion pairs, which can substitute for a hydrogen bonded $F^-{-}H$ "pair". Such interfacial ion pairing interactions are rarely observed in the other halide systems. This is quantitatively illustrated in Figure 9, which shows the probability distribution for the number of sodium ions coordinating F^- and Cl^-; larger anions are qualitatively similar to Cl^-. Indeed, about 90% of Cl^- ions do not have a sodium in their first coordination shell. In contrast, fluoride has nearly equal probabilities of being paired or unpaired with sodium and is even found in larger clusters

DOI: 10.1021/acs.jpcc.9b03054
J. Phys. Chem. C 2019, 123, 15618−15628

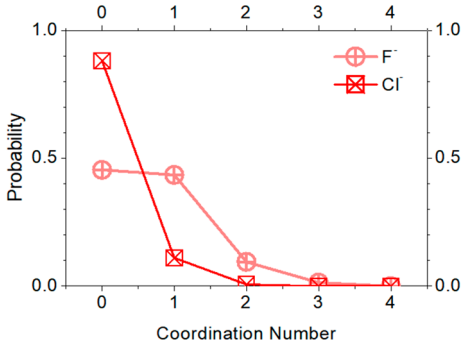

Figure 9. Probability distributions of coordination number between halides and their counterion Na^+.

with significant probability. Such clusters are readily observed in the snapshots shown in Figure 7a.

The surface Al−O−H bending potential is essential to correctly describe ion adsorption (see Supporting Information). This bending term ensures that the surface OH groups are either "in-plane" or "out-of-plane"; without such restriction, the surface OH groups may not point in the direction orthogonal to the surface to donate H-bonds. This suggests that the angle bending term strongly affects the interfacial properties and should not be neglected.

Impact of Ion Adsorption on Alumina Surface Structure. Upon adsorption of ions to the interface, the global distribution of alumina hydroxyl group orientations does not change, evidenced by the surface OH orientation distribution shown in Figure 10a. However, the coordination of ions to the hydroxyl groups locally impacts the surface OH orientation (Figure 7). To quantitatively illustrate this point, the joint probability of $P(\theta_{OH}$, "BM") is calculated, where "BM" stands for a specific bonding mode.

In the absence of salt, the surface OH orientation distribution can be decomposed into hydroxyls that accept or donate H-bonds with water, or free surface OH groups. The out-of-plane surface OH groups (peaks at 20°, Figure 10b) can donate H-bonds (D) to water, while the in-plane groups (peaks at 90°, Figure 10b) accept H-bonds from water molecules (A). This is consistent with the interpretation of interface-specific vibrational spectroscopy, which suggests that the H-bonds donated from water to in-plane surface OH groups are strong and result in low frequency (3000−3200 cm^{-1}) stretches in the vibrational SFG spectra of this interface.[12,17,19,61,85] On the other hand, the H-bonds donated from out-of-plane OH groups to water are relatively weaker.[12,13,85−87]

Among both OH group orientations, some do not form any H-bonds with water molecules and are marked as "Free" in Figure 10c. This significant population of free OH groups is consistent with a high frequency (free OH) peak in the vibrational SFG spectra of the water/alumina interface[85,86] and its assignment to aluminol groups.[12,13] The probability for surface OH groups donating and accepting hydrogen bonds at the same times, marked as "A+D" in Figure 10b, is very close to 0, which is consistent with previous AIMD simulations.[88]

In the presence of ions, OH groups can also interact with ions and thereby alter the decomposition of the probability distribution. The in-plane OH groups coordinate Na^+ with high affinity, resulting in nearly no free in-plane OH groups. Anions, F^- in Figure 10c, can coordinate with the out-of-plane OH groups, but some out-of-plane free OH groups remain, consistent with the presence of a free OH peak in the vibrational SFG spectra of aqueous salt solutions at the alumina surface.[85] The probability decomposition for NaCl is qualitatively similar to that for NaF (Figure S3). These local structural changes induced by adsorbates on the surface can be leveraged in heterogeneous nucleation and growth,[89] catalysis,[6,90] and templated self-assembly.[91,92]

Impact of Ion Adsorption on Interfacial Water Structure. The adsorption of ions can influence the structure of water at the interface. This structural change is quantified through the nonuniform, Z-dependent water density, as well as the orientation of interfacial water molecules. The water density, shown in Figure 11, exhibits a pronounced peak at Z = 0.26 nm corresponding to the first layer of water at the alumina surface. The density exhibits several increasingly less pronounced peaks at larger Z, indicating layering at the interface, before reaching the bulk value. As a reference, the water density profile from AIMD simulations is calculated and it is in good agreement with classical simulations, indicating the accuracy of the modeling of this work.

In the presence of ions, the first peak in the density is lower in height and broader than that of the pure water system (Figure 11). Interfacially adsorbed ions can replace water

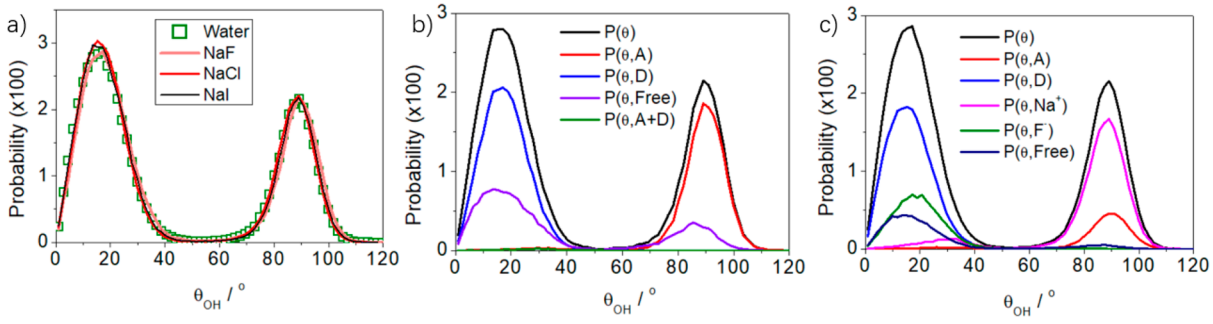

Figure 10. Comparison of the surface OH orientation distributions. (a) Total distribution, $P(\theta_{OH})$, for simulations of water only and water with ions, indicating that ion adsorption does not change the surface OH orientation distribution. (b) Decomposition of the $P(\theta_{OH})$ in the simulation of water and the surface only with respect to different bonding modes. "A" stands for the surface OH group that accepts hydrogen bonds from water; "D" stands for the surface OH group that donates hydrogen bonds to water, "A+D" stands for the surface OH group that donates and accepts hydrogen bonds with water at the same time and "Free" stands for the surface OH group does not have hydrogen bonds with water. (c) Decomposition of the $P(\theta_{OH})$ in the simulation in the presence of NaF. Bonding modes marks "Na^+" and "F^-" means that the surface OH group coordinates with Na^+ or donates hydrogen bond to F^-, respectively.

DOI: 10.1021/acs.jpcc.9b03054
J. Phys. Chem. C 2019, 123, 15618−15628

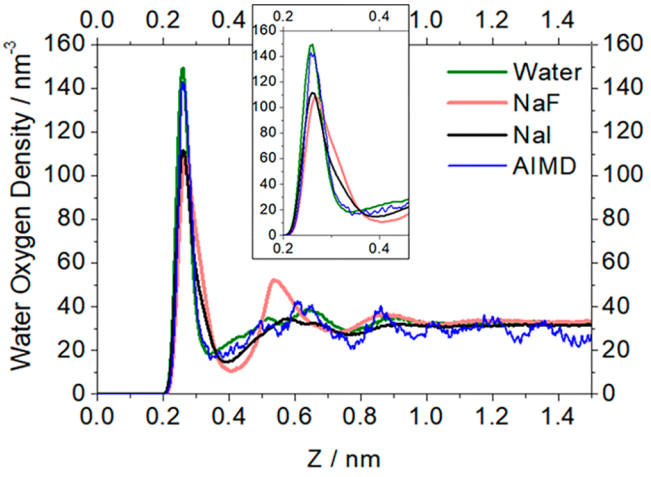

Figure 11. Water density profile near the interface for neat water and in the presence of various sodium halides. The water density is estimated by the number density of water oxygen atoms. For clarity, results from simulations with NaCl and NaBr are shown in Supporting Information.

molecules H-bonded to the surface, as described above. Water molecules in the hydration shells of the resulting adsorbed Na^+ lead to a shoulder in the high Z side of the first peak in the density (details will be discussed in next section).

This is evidenced by the joint probability density, $\rho(Z,\theta_\mu)$, in Figure 12a, for a water molecule to be at a distance Z from the

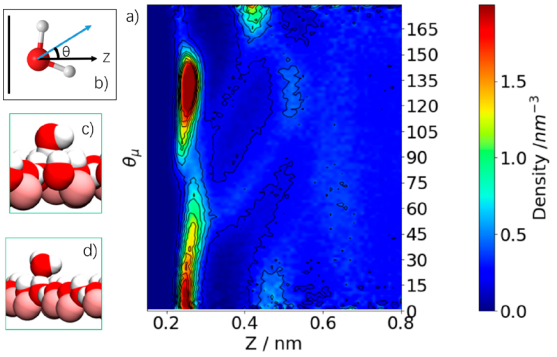

Figure 12. (a) Joint probability density, $\rho(Z,\theta_\mu)$ calculated from simulations with solid surface and only water. Here, only the region of 0.15−0.8 nm from the solid is shown. (b) Definition of θ_μ. (c) Snapshot of an interfacial water molecule donating a H-bond to the surface OH. (d) Snapshot of interfacial water accepting H-bonds from the surface OH.

surface with an orientational angle θ_μ, where θ_μ is the angle between water dipole vector and the surface normal (Z axis, Figure 12b). Within the first interfacial layer, water molecules show two major populations, in agreement with ab initio MD simulations.[88] The predominant orientation, the peak near θ_μ = 130°, corresponds to water molecules that donate H-bonds to the surface (Figure 12c), while the lesser, but still significant population, peaked at θ_μ = 0°, corresponds to water molecules that accept H-bonds from the out-of-plane surface hydroxyl groups (Figure 12d). The broadness of this acceptor peak arises from the "delocalized" picture of lone pairs implicitly assumed in the SPC/E model of water. A water model with more localized lone pairs, such as TIP5P, would lead to a narrower, but qualitatively similar peak at low θ_μ.[93,94] Some

significant orientational ordering remains in the second water layer, with populations at θ_μ = 180° and θ_μ = 0°. Beyond this layer, significant orientational ordering is not observed.

Ion adsorption also impacts the orientational structure of interfacial water, in addition to the translational ordering discussed above. Upon addition of salt, Figure 13, the peak

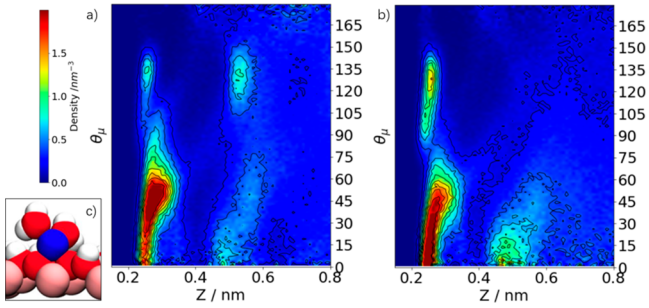

Figure 13. Joint probability density, $\rho(Z,\theta_\mu)$ calculated from simulations with (a) NaF or (b) NaI. (c) Snapshot of the solvation shell of surface bonded Na^+.

near 130° almost disappears, suggesting that the strong water−surface H-bonds are replaced with strong sodium−surface electrostatic interactions. The dominant population of interfacial water orientations is instead centered around θ_μ = 45°. This peak is also located at a slightly larger distance from the surface than in the pure water case and arises from water molecules in the hydration shell of Na^+ adsorbed directly to the surface (Figure 13c). The joint probability densities for NaF and NaI solutions are qualitatively similar within the first water layer, although the peak near 130° is larger in the case of NaI, because there are less sodium ions adsorbed to the surface. Significant differences arise in the second layer of water, and the origins of these differences will be discussed below.

Differences in the Z-dependent orientational order of water among the various systems are more readily observed through examination of the orientational density

$$\Theta(Z) = \int_0^\pi \rho(Z, \theta_\mu) \sin\theta_\mu \cos\theta_\mu \, d\theta_\mu = \rho(Z)\langle\cos\theta_\mu(Z)\rangle \tag{2}$$

as well as the average orientation, $\langle\cos\theta_\mu(Z)\rangle$, which is widely reported to study interfacial water orientation and spectra

$$\langle\cos\theta_\mu(Z)\rangle = \frac{\Theta(z)}{\int_0^\pi \rho(Z, \theta_\mu) \sin\theta_\mu \, d\theta_\mu} = \frac{\Theta(z)}{\rho(Z)} \tag{3}$$

which are shown in parts (a) and (b) of Figure 14, respectively.

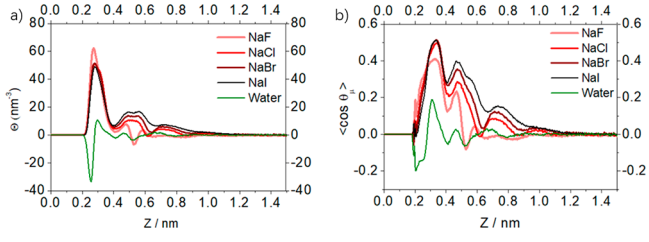

Figure 14. Water orientational ordering as characterized by (a) the density $\Theta(Z)$ as defined in eq 2 and (b) $\langle\cos\theta_\mu(Z)\rangle$.

DOI: 10.1021/acs.jpcc.9b03054
J. Phys. Chem. C 2019, 123, 15618−15628

In the absence of salt, the large population of water molecules at high θ_μ near the surface leads to the large negative peak in both functions, and the subsequent ordering of further layers leads to the damped oscillations in both $\Theta(Z)$ and $\langle\cos\theta_\mu(Z)\rangle$, which decay to zero in less than 1 nm. This small decay length is not surprising because the α-alumina(0001) surface model in this work is neutral, and the surface dipole can be completely screened by water over a short distance. In the presence of salt, both $\Theta(Z)$ and $\langle\cos\theta_\mu(Z)\rangle$ are positive for nearly all Z, with the exception of small peaks near 0.5 and 0.6 nm NaF and NaCl systems. Moreover, this ordering persists to at least 1 nm for the NaCl, NaBr, and NaI systems, such that these salts increase the width of the water/alumina interface. The orientational ordering of water in the NaF system decays over the same length scale as the pure water system.

To understand the screening behavior that leads to these different decay lengths, the electric field generated at the interface and its contributions from the various components of the system are examined (shown in the Supporting Information). Ion adsorption creates a positive electric field (pointing away from the surface) due to the excess Na^+ at the surface. To screen this field, water molecules reorient their dipoles to point toward the solid surface, creating a negative electric field that partially screens the one generated by the positive Na^+. Adsorbed anions will also screen this positive field. This screening is achieved more readily with fluoride, which adsorbs more readily to the interface than the other anions studied here, evidenced by the large second peaks in the fluoride density profiles. This strong adsorption screens the interfacial electric field within the first few layers, resulting in a small decay length for the orientational order.

The larger anions display larger values of $\Theta(Z)$ and $\langle\cos\theta_\mu(Z)\rangle$, especially after the first layer. The largest anion, I^-, adsorbs the least but has the largest $\Theta(Z)$ and $\langle\cos\theta_\mu(Z)\rangle$ (Figure 14), indicating that interfacial water is ordered the most in this system. Because I^- has the weakest adsorption, it also exhibits the weakest screening of the interfacial electric field. Thus, this electric field can extend out to longer distances, ordering water on a larger length scale. These differences in screening and the resulting changes in the size of the interfacially ordered region contribute to differences measured in interfacial spectroscopy of these systems.

CONCLUSION

In this work, ion adsorption and water behavior at the neutral α-alumina(0001)/water interface are investigated by classical MD simulations in the presence and absence of sodium halides. Several surface models based on CLAYFF are tested, and simulations with a flexible solid surface model and the inclusion of the surface Al−O−H bending potential yield an accurate description of the surface OH angle distribution, water density profile, and electron density profile, as compared to AIMD simulations and experimental estimates. Holding the surface rigid, as is often done in MD simulations, as well as omitting the Al−O−H bending potential, can significantly impact interfacial properties, including ion adsorption, and we suggest that surface flexibility and Al−O−H bending potentials should be included in MD simulations to yield accurate predictions.

In the simulations of aqueous sodium halide solutions, halide ion adsorption follows the ion charge density, $F^- > Cl^- > Br^- > I^-$, and adsorption of Na^+ enhances anion adsorption to this interface. The large predicted adsorption of F^- is also in good quantitative agreement with experiments, supporting that the model in this work yields a reasonable description of the alumina-aqueous electrolyte interface. Both Na^+ and F^- show high affinity, with a local density greater than 10 times the bulk value due to (1) the specific hexagonal surface OH pattern of the α-alumina (0001), (2) the coordination of Na^+ by three surface oxygen atoms, (3) hydrogen bonds between F^- and the surface, and (4) the Na^+−F^- ion pairing. However, ion pairing at the interface between Na^+ and other halides is observed with lower probability. The ion adsorption also affects the local orientation of surface OH groups; however, the global distribution of the surface OH orientation is not affected by ion adsorption.

The excess Na^+ near the interface changes the hydrogen bonding structure of interfacial water molecules. Adsorbed Na^+ displaces interfacial waters, decreasing the population of H-bond donors to surface hydroxyl groups, in addition to bring some of the Na^+ hydration shell into the interfacial region. These two effects change the net interfacial water orientation and produce an ordering that persists over a distance of about 1 nm from the solid surface. In addition, I^- has the lowest adsorption, but the largest effect on orientation, due to the weak screening ability of I^-.

In summary, this work provides a detailed picture of ion adsorption near the interface and reveals microscopic structural information that we hope will help researchers understand water/solid interfacial behavior. In particular, the molecular-scale characterization of interfacial water and surface hydroxyl group orientation and hydrogen-bonding structure aids in the interpretation of interface-specific spectroscopic studies.[12] Moreover, understanding the basic physical chemistry underlying the adsorption of charged groups to mineral surfaces should generalize to electrostatically driven biomolecular adsorption and adhesion processes. For example, recent work has suggested that cation adsorption to surfaces facilitates the adsorption of anionic C-termini of peptides,[80,81,95] in much the same way that sodium adsorption is found to enhance anion adsorption here. Finally, ion adsorption can create local structural patterning at mineral surfaces and may be particularly useful in guiding interfacial assembly and catalysis. One can envision using these interfacial liquid-induced surface perturbations to control important length scales, hydrogen bonding, and intermolecular arrangements in surface-driven assemblies and chemical reactions.

ASSOCIATED CONTENT

Supporting Information

The Supporting Information is available free of charge on the ACS Publications website at DOI: 10.1021/acs.jpcc.9b03054.

Comparison of solid relaxation, water density profile of all simulations, impact of the Al−O−H angle bending potential on ion adsorption, comparison of the surface OH orientation distribution of NaF and NaCl, and electric field profile of NaF and NaI (PDF)

AUTHOR INFORMATION

Corresponding Authors

*(E.B.) E-mail: eborguet@temple.edu.

*(V.C.) E-mail: vincenzo.carnevale@temple.edu.

ORCID

Ruiyu Wang: 0000-0003-1608-140X

DOI: 10.1021/acs.jpcc.9b03054
J. Phys. Chem. C 2019, 123, 15618−15628

Mark DelloStritto: 0000-0002-0678-5860
Richard C. Remsing: 0000-0002-0922-4882
Vincenzo Carnevale: 0000-0002-1918-8280

Notes

The authors declare no competing financial interest.

■ ACKNOWLEDGMENTS

This work was supported as part of the Center for Complex Materials from First-Principles (CCM), an Energy Frontier Research Center funded by the U.S. Department of Energy, Office of Science, Basic Energy Sciences, under Award #DE-SC0012575. This research includes calculations carried out on Temple University's HPC resources and thus was supported in part by the National Science Foundation through major research instrumentation Grant Number 1625061 and by the US Army Research Laboratory under Contract Number W911NF-16-2-0189. R.W. thanks Temple University for a Presidential Fellowship. M.D.S. thanks the Computational Chemical Center: Chemistry in Solution and at Interfaces funded by the DOE under Award DE-SC0019394. M.L.K. thanks H. H. Sheikh Saud bin Saqr al Qasimi for the award of a Sheikh Saqr Research Fellowship.

■ REFERENCES

(1) Polly, R.; Schimmelpfennig, B.; Flörsheimer, M.; Kruse, K.; AbdElMonem, A.; Klenze, R.; Rauhut, G.; Fanghänel, T. Theoretical Investigation of the Water/Corundum (0001) Interface. *J. Chem. Phys.* **2009**, *130*, No. 064702.

(2) Thenuwara, A. C.; Cerkez, E. B.; Shumlas, S. L.; Attanayake, N. H.; McKendry, I. G.; Frazer, L.; Borguet, E.; Kang, Q.; Remsing, R. C.; Klein, M. L.; et al. Nickel Confined in the Interlayer Region of Birnessite: an Active Electrocatalyst for Water Oxidation. *Angew. Chem., Int. Ed.* **2016**, *55*, 10381−10385.

(3) Arrouvel, C.; Diawara, B.; Costa, D.; Marcus, P. DFT Periodic Study of the Adsorption of Glycine on the Anhydrous and Hydroxylated (0001) Surfaces of α-Alumina. *J. Phys. Chem. C* **2007**, *111*, 18164−18173.

(4) Tougerti, A.; Methivier, C.; Cristol, S.; Tielens, F.; Che, M.; Carrier, X. Structure of Clean and Hydrated α-Al_2O_3 ($1\bar{1}02$) Surfaces: Implication on Surface Charge. *Phys. Chem. Chem. Phys.* **2011**, *13*, 6531−6543.

(5) Moustafa, A. B.; Abdel-Latif, Z. H.; Amer, L. I.; Sayyah, S. M. Aqueous Polymerization of Methyl Methacrylate Catalyzed by Corundum and Characterization of the Obtained Polymers. *J. Polym. Sci., Part A: Polym. Chem.* **1986**, *24*, 3049−3056.

(6) Kitadai, N.; Oonishi, H.; Umemoto, K.; Usui, T.; Fukushi, K.; Nakashima, S. Glycine Polymerization on Oxide Minerals. *Origins Life Evol. Biospheres* **2017**, *47*, 123−143.

(7) Meenakshi; Maheshwari, R. C. Fluoride in Drinking Water and its Removal. *J. Hazard. Mater.* **2006**, *137*, 456−463.

(8) Hudson, L. K.; Misra, C.; Perrotta, A. J.; Wefers, K.; Williams, F. S. Aluminum Oxide. *Ullmann's Encyclopedia of Industrial Chemistry* **2000**, DOI: 10.1002/14356007.a01_557.

(9) Björneholm, O.; Hansen, M. H.; Hodgson, A.; Liu, L.-M.; Limmer, D. T.; Michaelides, A.; Pedevilla, P.; Rossmeisl, J.; Shen, H.; Tocci, G.; et al. Water at Interfaces. *Chem. Rev.* **2016**, *116*, 7698−7726.

(10) Ma, S.-Y.; Liu, L.-M.; Wang, S.-Q. Water Film Adsorbed on the α-Al_2O_3(0001) Surface: Structural Properties and Dynamical Behaviors from First-Principles Molecular Dynamics Simulations. *J. Phys. Chem. C* **2016**, *120*, 5398−5409.

(11) Huang, P.; Pham, T. A.; Galli, G.; Schwegler, E. Alumina-(0001)/Water Interface: Structural Properties and Infrared Spectra from First-Principles Molecular Dynamics Simulations. *J. Phys. Chem. C* **2014**, *118*, 8944−8951.

(12) DelloStritto, M.; Sofo, J. Bond Polarizability Model for Sum Frequency Generation at the Al_2O_3(0001)−H_2O Interface. *J. Phys. Chem. A* **2017**, *121*, 3045−3055.

(13) DelloStritto, M.; Piontek, S. M.; Klein, M. L.; Borguet, E. Relating Interfacial Order to Sum Frequency Generation with Ab Initio Simulations of the Aqueous Al_2O_3(0001) and ($11\bar{2}0$) Interfaces. *J. Phys. Chem. C* **2018**, *122*, 21284−21294.

(14) Catalano, J. G. Weak Interfacial Water Ordering on Isostructural Hematite and Corundum (0 0 1) Surfaces. *Geochim. Cosmochim. Acta* **2011**, *75*, 2062−2071.

(15) Argyris, D.; Phan, A.; Striolo, A.; Ashby, P. D. Hydration Structure at the α-Al_2O_3 (0001) Surface: Insights from Experimental Atomic Force Spectroscopic Data and Atomistic Molecular Dynamics Simulations. *J. Phys. Chem. C* **2013**, *117*, 10433−10444.

(16) Tuladhar, A.; Dewan, S.; Kubicki, J. D.; Borguet, E. Spectroscopy and Ultrafast Vibrational Dynamics of Strongly Hydrogen Bonded OH Species at the α-Al_2O_3 ($11\bar{2}0$)/H_2O Interface. *J. Phys. Chem. C* **2016**, *120*, 16153−16161.

(17) Tuladhar, A.; Piontek, S. M.; Borguet, E. Insights on Interfacial Structure, Dynamics, and Proton Transfer from Ultrafast Vibrational Sum Frequency Generation Spectroscopy of the Alumina(0001)/Water Interface. *J. Phys. Chem. C* **2017**, *121*, 5168−5177.

(18) Sung, J.; Zhang, L.; Tian, C.; Waychunas, G. A.; Shen, Y. R. Surface Structure of Protonated R-Sapphire ($1\bar{1}02$) Studied by Sum-Frequency Vibrational Spectroscopy. *J. Am. Chem. Soc.* **2011**, *133*, 3846−3853.

(19) Zhang, L.; Tian, C.; Waychunas, G. A.; Shen, Y. R. Structures and Charging of α-Alumina (0001)/Water Interfaces Studied by Sum-Frequency Vibrational Spectroscopy. *J. Am. Chem. Soc.* **2008**, *130*, 7686−7694.

(20) Quezada, G. R.; Rozas, R. E.; Toledo, P. G. Molecular Dynamics Simulations of Quartz (101)−Water and Corundum (001)−Water Interfaces: Effect of Surface Charge and Ions on Cation Adsorption, Water Orientation, and Surface Charge Reversal. *J. Phys. Chem. C* **2017**, *121*, 25271−25282.

(21) Xu, T.; Stubbs, J. E.; Eng, P. J.; Catalano, J. G. Response of Interfacial Water to Arsenate Adsorption on Corundum (0 0 1) Surfaces: Effects of pH and Adsorbate Surface Coverage. *Geochim. Cosmochim. Acta* **2018**, *239*, 198−212.

(22) Hass, K. C.; Schneider, W. F.; Curioni, A.; Andreoni, W. The Chemistry of Water on Alumina Surfaces: Reaction Dynamics from First Principles. *Science* **1998**, *282*, 265−268.

(23) Lutterotti, L.; Scardi, P. Simultaneous Structure and Size-strain Refinement by the Rietveld Method. *J. Appl. Crystallogr.* **1990**, *23*, 246−252.

(24) Abraham, M. J.; Murtola, T.; Schulz, R.; Páll, S.; Smith, J. C.; Hess, B.; Lindahl, E. J. S. GROMACS: High Performance Molecular Simulations Through Multi-level Parallelism from Laptops to Supercomputers. *SoftwareX* **2015**, *1*, 19−25.

(25) Pronk, S.; Páll, S.; Schulz, R.; Larsson, P.; Bjelkmar, P.; Apostolov, R.; Shirts, M. R.; Smith, J. C.; Kasson, P. M.; Van Der Spoel, D.; et al. GROMACS 4.5: a High-throughput and Highly Parallel Open Source Molecular Simulation Toolkit. *Bioinformatics* **2013**, *29*, 845−854.

(26) Berendsen, H. J. C.; van der Spoel, D.; van Drunen, R. GROMACS: A Message-passing Parallel Molecular Dynamics Implementation. *Comput. Phys. Commun.* **1995**, *91*, 43−56.

(27) Pall, S.; Abraham, M. J.; Kutzner, C.; Hess, B.; Lindahl, E. Tackling Exascale Software Challenges in Molecular Dynamics Simulations with GROMACS. *Lecture Notes in Computer Science* **2015**, *8759*, 3−27.

(28) Hess, B.; Kutzner, C.; van der Spoel, D.; Lindahl, E. GROMACS 4: Algorithms for Highly Efficient, Load-Balanced, and Scalable Molecular Simulation. *J. Chem. Theory Comput.* **2008**, *4*, 435−447.

(29) Van Der Spoel, D.; Lindahl, E.; Hess, B.; Groenhof, G.; Mark, A. E.; Berendsen, H. J. C. GROMACS: Fast, Flexible, and Free. *J. Comput. Chem.* **2005**, *26*, 1701−1718.

DOI: 10.1021/acs.jpcc.9b03054
J. Phys. Chem. C 2019, 123, 15618−15628

(30) Lindahl, E.; Hess, B.; van der Spoel, D. GROMACS 3.0: a Package for Molecular Simulation and Trajectory Analysis. *J. Mol. Model.* **2001**, *7*, 306−317.
(31) Cygan, R. T.; Liang, J.-J.; Kalinichev, A. G. Molecular Models of Hydroxide, Oxyhydroxide, and Clay Phases and the Development of a General Force Field. *J. Phys. Chem. B* **2004**, *108*, 1255−1266.
(32) Horinek, D.; Mamatkulov, S. I.; Netz, R. R. Rational Design of Ion Force Fields Based on Thermodynamic Solvation Properties. *J. Chem. Phys.* **2009**, *130*, 124507.
(33) Berendsen, H. J. C.; Grigera, J. R.; Straatsma, T. P. The Missing Term in Effective Pair Potentials. *J. Phys. Chem.* **1987**, *91*, 6269−6271.
(34) Hess, B. P-LINCS: A Parallel Linear Constraint Solver for Molecular Simulation. *J. Chem. Theory Comput.* **2008**, *4*, 116−122.
(35) Parrinello, M.; Rahman, A. Polymorphic Transitions in Single Crystals: A New Molecular Dynamics Method. *J. Appl. Phys.* **1981**, *52*, 7182−7190.
(36) Nosé, S.; Klein, M. L. Constant Pressure Molecular Dynamics for Molecular Systems. *Mol. Phys.* **1983**, *50*, 1055−1076.
(37) Nosé, S. A Molecular Dynamics Method for Simulations in the Canonical Ensemble. *Mol. Phys.* **1984**, *52*, 255−268.
(38) Hoover, W. G. Canonical Dynamics: Equilibrium Phase-space Distributions. *Phys. Rev. A: At., Mol., Opt. Phys.* **1985**, *31*, 1695−1697.
(39) Essmann, U.; Perera, L.; Berkowitz, M. L.; Darden, T.; Lee, H.; Pedersen, L. G. A Smooth Particle Mesh Ewald Method. *J. Chem. Phys.* **1995**, *103*, 8577−8593.
(40) Michaud-Agrawal, N.; Denning, E. J.; Woolf, T. B.; Beckstein, O. MDAnalysis: A Toolkit for the Analysis of Molecular Dynamics Simulations. *J. Comput. Chem.* **2011**, *32*, 2319−2327.
(41) Gowers, R.; Linke, M.; Barnoud, J.; Reddy, T. J. E.; Melo, M. N.; Seyler, S. L.; Domański, J.; Dotson, D. L.; Buchoux, S.; Kenney, I. M.; Beckstein, O. MDAnalysis: A Python Package for the Rapid Analysis of Molecular Dynamics Simulations. *Proceedings of the 15th Python in Science Conference* **2016**, 98−105.
(42) Torrie, G. M.; Valleau, J. P. Nonphysical Sampling Distributions in Monte Carlo Free-energy Estimation: Umbrella Sampling. *J. Comput. Phys.* **1977**, *23*, 187−199.
(43) Tribello, G. A.; Bonomi, M.; Branduardi, D.; Camilloni, C.; Bussi, G. PLUMED 2: New Feathers for an Old Bird. *Comput. Phys. Commun.* **2014**, *185*, 604−613.
(44) Tan, Z.; Gallicchio, E.; Lapelosa, M.; Levy, R. M. Theory of Binless Multi-state Free Energy Estimation with Applications to Protein-ligand Binding. *J. Chem. Phys.* **2012**, *136*, 144102.
(45) Humphrey, W.; Dalke, A.; Schulten, K. VMD: Visual Molecular Dynamics. *J. Mol. Graphics* **1996**, *14*, 33−38.
(46) Giannozzi, P.; Andreussi, O.; Brumme, T.; Bunau, O.; Buongiorno Nardelli, M.; Calandra, M.; Car, R.; Cavazzoni, C.; Ceresoli, D.; Cococcioni, M.; et al. Advanced Capabilities for Materials Modelling with Quantum ESPRESSO. *J. Phys.: Condens. Matter* **2017**, *29*, 465901.
(47) Giannozzi, P.; Baroni, S.; Bonini, N.; Calandra, M.; Car, R.; Cavazzoni, C.; Ceresoli, D.; Chiarotti, G. L.; Cococcioni, M.; Dabo, I.; et al. QUANTUM ESPRESSO: a Modular and Open-source Software Project for Quantum Simulations of Materials. *J. Phys.: Condens. Matter* **2009**, *21*, 395502.
(48) Vanderbilt, D. Optimally Smooth Norm-conserving Pseudopotentials. *Phys. Rev. B: Condens. Matter Mater. Phys.* **1985**, *32*, 8412−8415.
(49) Sun, J.; Ruzsinszky, A.; Perdew, J. P. Strongly Constrained and Appropriately Normed Semilocal Density Functional. *Phys. Rev. Lett.* **2015**, *115*, No. 036402.
(50) Sun, J.; Remsing, R. C.; Zhang, Y.; Sun, Z.; Ruzsinszky, A.; Peng, H.; Yang, Z.; Paul, A.; Waghmare, U.; Wu, X.; et al. Accurate First-Principles Structures and Energies of Diversely Bonded Systems from an Efficient Density Functional. *Nat. Chem.* **2016**, *8*, 831.
(51) Chen, M.; Ko, H.-Y.; Remsing, R. C.; Calegari Andrade, M. F.; Santra, B.; Sun, Z.; Selloni, A.; Car, R.; Klein, M. L.; Perdew, J. P. Ab Initio Theory and Modeling of Water. *Proc. Natl. Acad. Sci. U. S. A.* **2017**, *114*, 10846.
(52) DelloStritto, M. J.; Piontek, S. M.; Klein, M. L.; Borguet, E. Effect of Functional and Electron Correlation on the Structure and Spectroscopy of the $Al_2O_3(001)-H_2O$ Interface. *J. Phys. Chem. Lett.* **2019**, *10*, 2031−2036.
(53) Soares, E. A.; Van Hove, M. A.; Walters, C. F.; McCarty, K. F. Structure of the $\alpha-Al_2O_3(0001)$ Surface from Low-energy Electron Diffraction: Al Termination and Evidence for Anomalously Large Thermal Vibrations. *Phys. Rev. B: Condens. Matter Mater. Phys.* **2002**, *65*, 195405.
(54) Elam, J. W.; Nelson, C. E.; Cameron, M. A.; Tolbert, M. A.; George, S. M. Adsorption of H_2O on a Single-crystal α-$Al_2O_3(0001)$ Surface. *J. Phys. Chem. B* **1998**, *102*, 7008−7015.
(55) Eng, P. J.; Trainor, T. P.; Brown, G. E., Jr.; Waychunas, G. A.; Newville, M.; Sutton, S. R.; Rivers, M. L. Structure of the Hydrated α-Al_2O_3 (0001) Surface. *Science* **2000**, *288*, 1029−1033.
(56) Liu, P.; Kendelewicz, T.; Brown, G. E.; Nelson, E. J.; Chambers, S. A. Reaction of Water Vapor with α-$Al_2O_3(0001)$ and α-$Fe_2O_3(0001)$ Surfaces: Synchrotron X-ray Photoemission Studies and Thermodynamic Calculations. *Surf. Sci.* **1998**, *417*, 53−65.
(57) Barth, C.; Reichling, M. Imaging the Atomic Arrangements on the High-temperature Reconstructed α-$Al_2O_3(0001)$ Surface. *Nature* **2001**, *414*, 54.
(58) Hass, K. C.; Schneider, W. F.; Curioni, A.; Andreoni, W. First-Principles Molecular Dynamics Simulations of H_2O on α-Al_2O_3 (0001). *J. Phys. Chem. B* **2000**, *104*, 5527−5540.
(59) Franks, G. V.; Gan, Y. Charging Behavior at the Alumina−Water Interface and Implications for Ceramic Processing. *J. Am. Ceram. Soc.* **2007**, *90*, 3373−3388.
(60) Glatz, B.; Sarupria, S. Heterogeneous Ice Nucleation: Interplay of Surface Properties and Their Impact on Water Orientations. *Langmuir* **2018**, *34*, 1190.
(61) Gaigeot, M.-P.; Sprik, M.; Sulpizi, M. Oxide/Water Interfaces: How the Surface Chemistry Modifies Interfacial Water Properties. *J. Phys.: Condens. Matter* **2012**, *24*, 124106.
(62) Wilson, M. A.; Pohorille, A.; Pratt, L. R. Surface Potential of the Water Liquid−Vapor Interface. *J. Chem. Phys.* **1988**, *88*, 3281−3285.
(63) Remsing, R. C.; Weeks, J. D. Hydrophobicity Scaling of Aqueous Interfaces by an Electrostatic Mapping. *J. Phys. Chem. B* **2015**, *119*, 9268−9277.
(64) Fenter, P.; Kerisit, S.; Raiteri, P.; Gale, J. D. Is the Calcite−Water Interface Understood? Direct Comparisons of Molecular Dynamics Simulations with Specular X-ray Reflectivity Data. *J. Phys. Chem. C* **2013**, *117*, 5028−5042.
(65) Jungwirth, P.; Tobias, D. J. Molecular Structure of Salt Solutions: A New View of the Interface with Implications for Heterogeneous Atmospheric Chemistry. *J. Phys. Chem. B* **2001**, *105*, 10468−10472.
(66) Jungwirth, P.; Tobias, D. J. Ions at the Air/Water Interface. *J. Phys. Chem. B* **2002**, *106*, 6361−6373.
(67) Jungwirth, P.; Tobias, D. J. Specific Ion Effects at the Air/Water Interface. *Chem. Rev.* **2006**, *106*, 1259−1281.
(68) Horinek, D.; Netz, R. R. Specific Ion Adsorption at Hydrophobic Solid Surfaces. *Phys. Rev. Lett.* **2007**, *99*, 226104.
(69) Tobias, D. J.; Stern, A. C.; Baer, M. D.; Levin, Y.; Mundy, C. J. Simulation and Theory of Ions at Atmospherically Relevant Aqueous Liquid-Air Interfaces. *Annu. Rev. Phys. Chem.* **2013**, *64*, 339−359.
(70) Jungwirth, P.; Winter, B. Ions at Aqueous Interfaces: From Water Surface to Hydrated Proteins. *Annu. Rev. Phys. Chem.* **2008**, *59*, 343−366.
(71) Horinek, D.; Herz, A.; Vrbka, L.; Sedlmeier, F.; Mamatkulov, S. I.; Netz, R. R. Specific Ion Adsorption at the Air/Water Interface: The Role of Hydrophobic Solvation. *Chem. Phys. Lett.* **2009**, *479*, 173−183.
(72) Vembanur, S.; Venkateshwaran, V.; Garde, S. Structure and Dynamics of Single Hydrophobic/Ionic Heteropolymers at the Vapor−Liquid Interface of Water. *Langmuir* **2014**, *30*, 4654−4661.
(73) Otten, D. E.; Petersen, P. B.; Saykally, R. J. Observation of Nitrate Ions at the Air/Water Interface by UV-Second Harmonic Generation. *Chem. Phys. Lett.* **2007**, *449*, 261−265.

DOI: 10.1021/acs.jpcc.9b03054
J. Phys. Chem. C 2019, 123, 15618−15628

(74) Allen, H. C.; Casillas-Ituarte, N. N.; Sierra-Hernández, M. R.; Chen, X.; Tang, C. Y. Shedding Light on Water Structure at Air−Aqueous Interfaces: Ions, Lipids, and Hydration. *Phys. Chem. Chem. Phys.* **2009**, *11*, 5538−5549.
(75) Liu, D.; Ma, G.; Levering, L. M.; Allen, H. C. Vibrational Spectroscopy of Aqueous Sodium Halide Solutions and Air−Liquid Interfaces: Observation of Increased Interfacial Depth. *J. Phys. Chem. B* **2004**, *108*, 2252−2260.
(76) Vaitheeswaran, S.; Thirumalai, D. Hydrophobic and Ionic Interactions in Nanosized Water Droplets. *J. Am. Chem. Soc.* **2006**, *128*, 13490−13496.
(77) Remsing, R. C.; Weeks, J. D. Dissecting Hydrophobic Hydration and Association. *J. Phys. Chem. B* **2013**, *117*, 15479−15491.
(78) Andersen, H. C.; Weeks, J. D.; Chandler, D. Relationship between the Hard-Sphere Fluid and Fluids with Realistic Repulsive Forces. *Phys. Rev. A: At., Mol., Opt. Phys.* **1971**, *4*, 1597−1607.
(79) López Valdivieso, A.; Reyes Bahena, J. L.; Song, S.; Herrera Urbina, R. Temperature Effect on the Zeta Potential and Fluoride Adsorption at the α-Al_2O_3/Aqueous Solution Interface. *J. Colloid Interface Sci.* **2006**, *298*, 1−5.
(80) Pradier, C. M.; Humblot, V.; Stievano, L.; Méthivier, C.; Lambert, J. F. Salt Concentration and pH-Dependent Adsorption of Two Polypeptides on Planar and Divided Alumina Surfaces. *Langmuir* **2007**, *23*, 2463−2471.
(81) Costa, D.; Savio, L.; Pradier, C. M. Adsorption of Amino Acids and Peptides on Metal and Oxide Surfaces in Water Environment: A Synthetic and Prospective Review. *J. Phys. Chem. B* **2016**, *120*, 7039−7052.
(82) Luzar, A.; Chandler, D. Structure and Hydrogen Bond Dynamics of Water−dimethyl Sulfoxide Mixtures by Computer Simulations. *J. Chem. Phys.* **1993**, *98*, 8160−8173.
(83) Luzar, A.; Chandler, D. Hydrogen-bond Kinetics in Liquid Water. *Nature* **1996**, *379*, 55.
(84) Chowdhuri, S.; Chandra, A. Dynamics of Halide Ion−Water Hydrogen Bonds in Aqueous Solutions: Dependence on Ion Size and Temperature. *J. Phys. Chem. B* **2006**, *110*, 9674−9680.
(85) Tuladhar, A.; Piontek, S. M.; Frazer, L.; Borguet, E. Effect of Halide Anions on the Structure and Dynamics of Water Next to an Alumina (0001) Surface. *J. Phys. Chem. C* **2018**, *122*, 12819−12830.
(86) Abdelmonem, A.; Backus, E. H. G.; Bonn, M. Ice Nucleation at the Water−Sapphire Interface: Transient Sum-Frequency Response without Evidence for Transient Ice Phase. *J. Phys. Chem. C* **2018**, *122*, 24760−24764.
(87) Abdelmonem, A.; Backus, E. H. G.; Hoffmann, N.; Sánchez, M. A.; Cyran, J. D.; Kiselev, A.; Bonn, M. Surface-charge-induced Orientation of Interfacial Water Suppresses Heterogeneous Ice Nucleation on α-Alumina (0001). *Atmos. Chem. Phys.* **2017**, *17*, 7827−7837.
(88) Janeček, J.; Netz, R. R.; Flörsheimer, M.; Klenze, R.; Schimmelpfennig, B.; Polly, R. Influence of Hydrogen Bonding on the Structure of the (001) Corundum−Water Interface. Density Functional Theory Calculations and Monte Carlo Simulations. *Langmuir* **2014**, *30*, 2722−2728.
(89) Jun, Y.-S.; Kim, D.; Neil, C. W. Heterogeneous Nucleation and Growth of Nanoparticles at Environmental Interfaces. *Acc. Chem. Res.* **2016**, *49*, 1681−1690.
(90) Larmier, K.; Nicolle, A.; Chizallet, C.; Cadran, N.; Maury, S.; Lamic-Humblot, A.-F.; Marceau, E.; Lauron-Pernot, H. Influence of Coadsorbed Water and Alcohol Molecules on Isopropyl Alcohol Dehydration on γ-Alumina: Multiscale Modeling of Experimental Kinetic Profiles. *ACS Catal.* **2016**, *6*, 1905−1920.
(91) Park, S.; Lim, J.-H.; Chung, S.-W.; Mirkin, C. A. Self-Assembly of Mesoscopic Metal-Polymer Amphiphiles. *Science* **2004**, *303*, 348−351.
(92) Levchenko, I.; Bazaka, K.; Keidar, M.; Xu, S.; Fang, J. Hierarchical Multicomponent Inorganic Metamaterials: Intrinsically Driven Self-Assembly at the Nanoscale. *Adv. Mater.* **2018**, *30*, 1702226.
(93) Remsing, R. C.; Duignan, T. T.; Baer, M. D.; Schenter, G. K.; Mundy, C. J.; Weeks, J. D. Water Lone Pair Delocalization in Classical and Quantum Descriptions of the Hydration of Model Ions. *J. Phys. Chem. B* **2018**, *122*, 3519−3527.
(94) Remsing, R. C.; Baer, M. D.; Schenter, G. K.; Mundy, C. J.; Weeks, J. D. The Role of Broken Symmetry in Solvation of a Spherical Cavity in Classical and Quantum Water Models. *J. Phys. Chem. Lett.* **2014**, *5*, 2767−2774.
(95) Zheng, T.; Wu, C.; Chen, M.; Zhang, Y.; Cummings, P. T. Molecular Mechanics of the Cooperative Adsorption of a Pro-Hyp-Gly Tripeptide on a Hydroxylated Rutile TiO_2(110) Surface Mediated by Calcium Ions. *Phys. Chem. Chem. Phys.* **2016**, *18*, 19757−19764.

DOI: 10.1021/acs.jpcc.9b03054
J. Phys. Chem. C 2019, 123, 15618−15628